Analysis of Transient Magnetic Flux in Interpole of DC Motor Considering Hysteresis Phenomenon

By

Tsuguo ANDO* and Juro UMOTO*

(Received June 30, 1983)

Abstract

We first formulate a numerical calculation to solve the two-dimensional theoretical equations for an analysis of the transient response of the interpole flux in the dc motor. In this numerical calculation, the nodal method for considering Ampere's circuital law in space, and the Crank-Nicolson method for the time derivative are used. Next, we analyse the transient response of the magnetic flux, the distributions of the magnetic flux, and also the induced eddy current in the magnetic circuit simulating the interpole magnetic circuit in a dc motor, the yoke of which is constructed with a solid iron core. As a result, it is made clear that the interpole flux is delayed to the abrupt change of an armature current by the eddy current induced in the yoke. It is also clear that a large magnetic flux concentrates in the inner skin region of the yoke, because of the eddy current and the magnetic hysteresis. Moreover, it is noted that the distribution of the magnetic flux in the yoke is influenced very much by the conductivity of the yoke and the magnetic hysteresis.

Finally, we obtain a fairly good agreement between the calculated and the experimental results of the transient response of the magnetic flux.

1. Introduction

A direct current(dc) motor has a better speed-torque characteristic than an alternating current(ac) motor, and is widely applied to precise variable speed machines. However, in order to improve the superior characteristic, it is essential for the dc motor to maintain a good commutation. Even if a good commutation is held in steady driving, it often deteriorates in the case where a sudden change of an armature current occurs by a fluctuation of the load or the speed control. A commutation spark can occur in a serious case where the transitional delay of the response of the interpole flux to an armature current is brought about due to an induced eddy current in the magnetic circuit. Because the reactance voltage induced in commutation coils and

* Department of Electrical Engineering.

the counter magnetomotive force(mmf) due to the armature current are not compensated.

Many studies on the transient response of the interpole flux in small-sized motors, the yoke of which is usually constructed with solid core, have been reported. Those studies ware carried out mostly on the assumtion that the magnetic circuit in the dc motor can be simulated by a simplified magnetic circuit model with some constant permeability[1)~3)]. However, the actual dc motor has iron cores with a nonlinear permeability and a complex construction. Correspondingly, in order to analyse the flux response accurately, it is necessary to investigate the time behaviors of the flux distribution in the dc motor by using the nonlinear theory, considering the nonlinearity of the permeability.

In this paper, we first introduce some two-dimensional fundamental nonlinear equations to analyse the transient response of the magnetic flux. Then, we develop a numerical calculation for solving those equations, in which the nodal method considering Ampere's circuital law and the Crank-Nicolson method for the time derivative are used. In this analysis, not only the nonlinear permeability but also the hysteresis of the magnetic characteristic are considered. Next, applying the method to an appropriate magnetic circuit model of the interpole magnetic circuit, we examine the transient response of the interpole flux, the variation of the flux distribution etc. in a case where a rapid change of the armature current occurred.

2. Two-Dimensional Nodal Method for Numerical Solution of Magnetic Flux Distribution in Electric Machines

2.1 Fundamental equations

The magnetic flux distribution in electric machines can be obtained by solving the following Maxwell equations

$$\text{rot } \boldsymbol{H}=\boldsymbol{J},\ \text{rot } \boldsymbol{E}=-\partial \boldsymbol{B}/\partial t,\ \text{div } \boldsymbol{B}=0, \tag{1}$$

and the additional equations

$$\boldsymbol{B}=\mu \boldsymbol{H},\ \ \boldsymbol{J}=\boldsymbol{J}_s+\sigma \boldsymbol{E}. \tag{2}$$

In the equations, $\boldsymbol{B}$, $\boldsymbol{H}$, $\boldsymbol{E}$, μ and σ are the magnetic flux density, the magnetic field intensity, the electric field intensity, the permeability and the conductivity, respectively. $\boldsymbol{J}$ is the current density which is composed of the current density $\boldsymbol{J}_s$ supplied to the conductors of the exciting winding or the eddy current density $\sigma \boldsymbol{E}$ induced in iron cores. Here, we assume that the eddy current induced in the conductors is negligible compared with $\boldsymbol{J}_s$, and we also assume that the conductivity of the core is constant.

By using the magnetic vector potential $\boldsymbol{A}$ which satisfies $\boldsymbol{B}=\text{rot } \boldsymbol{A}$ and $\text{div } \boldsymbol{A}=0$,

Eqs. (1) and (2) can be transformed into the following equations, with respect to $\boldsymbol{A}$ and $\boldsymbol{J}_s$:

$$\text{rot}\ (\nu\ \text{rot}\ \boldsymbol{A}) = \boldsymbol{J}_s - \sigma\ \partial \boldsymbol{A}/\partial t,\ \text{div}\ \boldsymbol{A} = 0, \tag{3}$$

where $\nu = 1/\mu$ is the reciprocal permeability. Now, $\boldsymbol{B}$, $\boldsymbol{H}$ and $\boldsymbol{J}$ are expressed by

$$\boldsymbol{B} = \text{rot}\ \boldsymbol{A},\ \boldsymbol{H} = \nu\ \text{rot}\ \boldsymbol{A},\ \boldsymbol{J} = \boldsymbol{J}_s - \sigma\ \partial \boldsymbol{A}/\partial t. \tag{4}$$

If $\boldsymbol{A}$ is obtained by solving Eqs. (3) and (4), the magnetic flux ϕ passing through an arbitary cross-sectional area S with the contour C is obtainen by

$$\phi = \int_s \boldsymbol{B} \cdot d\boldsymbol{S} = \oint_c \boldsymbol{A} \cdot d\boldsymbol{l}. \tag{5}$$

For simplifying the analysis, let us investigate the two-dimensional flux distribution in an $x-y$ cross-section of the magnetic circuit. We assume that $\boldsymbol{B}$ and $\boldsymbol{H}$ don't vary in the z direction perpendicular to the cross-section, and that $\boldsymbol{A}$ and $\boldsymbol{J}_s$ have only their respective z components. Then, by using $\boldsymbol{A} = \boldsymbol{k}A(x, y, t) = \boldsymbol{k}A$ and $\boldsymbol{J}_s = \boldsymbol{k}J_s(x, y, t) = \boldsymbol{k}J_s$, Eqs. (3), (4), and (5) are reduced to the following two-dimensional equations:

$$\text{rot}\ (\nu\ \text{rot}\ \boldsymbol{k}A) = \boldsymbol{k}(J_s - \sigma\ \partial A/\partial t),\ \text{div}\ \boldsymbol{k}A = 0, \tag{6}$$

$$\left.\begin{aligned} &B_x = \partial A/\partial y,\ B_y = -\partial A/\partial x,\ H_x = \nu\ \partial A/\partial y,\ H_y = -\nu \partial\ A/\partial x, \\ &J = J_s - \sigma\ \partial A/\partial t, \end{aligned}\right\} \tag{7}$$

$$\phi = \oint_c \boldsymbol{k}A \cdot d\boldsymbol{l} = \oint_c A \cdot dz = \Delta A l_s. \tag{8}$$

In these equations, $\boldsymbol{k}$ is the fundamental unit vector in the z direction, B_x, B_y, H_x and H_y are the x and y components of $\boldsymbol{B}$ and $\boldsymbol{H}$, respectively, J is the z component of $\boldsymbol{J}$, ΔA is the difference of vector potentials at two arbitary points in the $x-y$ plane and l_s is the length of the magnetic circuit in the z direction.

2.2 Nodal method

The finite difference or the finite element method has been mainly used to obtain an approximate numerical solution of Eq. (6), under some given boundary conditions. Here, we use a nodal method to calculate the magnetic flux distribution. The region in which Eq. (6) should be solved is subdivided into a large number of trianglar elements, in which J_s, ν and σ can be assumed to be uniform. Then, Eq. (6) is transfomed to a simultaneous discrete nodal equation with an unknown vector potential at each vertex of every triangular element. Let us explain the nodal method in a case where the vector potential is expressed by a first order function of a position in each element.

In a triangular element e with nodes i, j and k as shown in Fig. 1, the vector potential $A=A_e$ is assumed to be given by a linear approximation as follows:

$$A_e=a_e+b_e x+c_e y, \tag{9}$$

where

$$\left.\begin{aligned}&\begin{bmatrix} a_e \\ b_e \\ c_e \end{bmatrix}=\frac{1}{D_e}\begin{bmatrix} a_i & a_j & a_k \\ b_i & b_j & b_k \\ c_i & c_j & c_k \end{bmatrix}\begin{bmatrix} \mathrm{A}_i \\ \mathrm{A}_j \\ \mathrm{A}_k \end{bmatrix},\\ &a_i=x_j y_k-x_k y_j,\quad b_i=y_j-y_k,\quad c_i=x_k-x_j,\quad \text{etc},\\ &D_e=a_i+a_j+a_k,\\ &A_m,\ x_m,\ y_m : A,\ x \text{ and } y \text{ at rode } m,\\ &m=i,\ j,\ k.\end{aligned}\right\} \tag{9}'$$

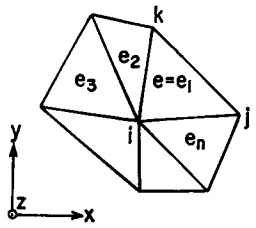

Fig. 1. Node i and its adjoining elements.

From Eqs. (7) and (9), the x and y components of $\boldsymbol{B}$ and $\boldsymbol{H}$ in element e are derived as follows:

$$\left.\begin{aligned}&\mathrm{B}_x=\frac{1}{D_e}\sum_{m=i}^{k} c_m A_m,\quad B_y=-\frac{1}{D_e}\sum_{m=i}^{k} b_m A_m,\\ &H_x=\frac{\nu_e}{D_e}\sum_{m=i}^{k} c_m A_m,\quad H_y=-\frac{\nu_e}{D_e}\sum_{m=i}^{k} b_m A_m,\end{aligned}\right\} \tag{10}$$

where $\nu=\nu_e$ is determined by the flux density $B_e=(B_x^2+B_y^2)^{1/2}$ and the magnetization curve of the material in element e. When the same expressions as Eqs. (9) and (10) are used for every element, the continuity of the normal component of $\boldsymbol{B}$ on a boundary line of two adjoining elements is maintained. On the other hand, the continuity of the tangential component of $\boldsymbol{H}$ along the boundary is not kept, and this is contrary to physical law. The nodal method is a superior numerical calculation, in which the boundary condition for $\boldsymbol{H}$ is replaced by Ampere's circuital law

$$\oint_c \boldsymbol{H}\cdot d\boldsymbol{l}=\int_s (J_s-\sigma\,\partial A/\partial t)\,dxdy \tag{11}$$

around each node. In this paper, the integration is carried out in the region, as shown by the broken line C in Fig. 2. In the figure, i', j' and k' are the middle points of three sides jk, ki and ij, respectively, and p is the outer center of element e.

Let us now derive a discrete nodal equation for node i. By using Eqs. (9), (10) and (11), we can obtain

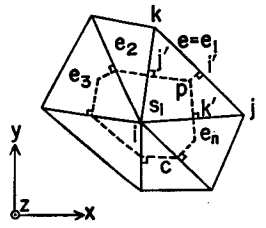

Fig. 2. Integral path C around i.

$$\int_{ik'pj'} \boldsymbol{H} \cdot d\boldsymbol{l} = \frac{\nu_e}{2D_e} \sum_{m=i}^{k} (c_i c_m + b_i b_m) A_m, \tag{12}$$

$$\int_{ik'pj'i} J_e dxdy = J_{se} S_i, \tag{13}$$

$$\int_{ik'pj'i} \left(\sigma \frac{\partial A}{\partial t}\right) dxdy = \sigma_e S_i \frac{\partial A_i}{\partial t}, \tag{14}$$

where

$$\left.\begin{aligned} &S_i = \frac{1}{16S_e}\left\{|b_i b_k + c_i c_k|\,(b_j^2 + c_j^2) + |b_i b_j + c_i c_j|\,(b_k^2 + c_k^2)\right\}, \\ &\frac{1}{4}S_e \leq S_i \leq \frac{1}{2}S_e. \end{aligned}\right\} \tag{15}$$

In these equations, Jse, ν_e and σ_e are the values of J_s, ν and σ in element e, respectively, and $S_e = D_e/2$ is the area of element e. Here, we must notice that the contributions of A_j and A_k are neglected in the integral result of Eq. (14)[4]. Also, when element e is an obtuse-angled triangle and the outer center lies outside the triangle, we put $S_i = S_e/2$ or $S_i = S_e/4$ into Eqs. (13) and (14) according to whether the vertical angle at node i is greater or smaller than $\pi/2$. In this connection, in the conventional nodal method[5], every element must be an acute-angled triangle. Hence, it is difficult to apply to a complex field region as in electric machines. Also, the finite element method, in which $S_i = S_e/3$ is substituted into Eqs. (13) and (14) instead of Eq. (15), has a weak point in treating the rectangular conductor carrying a uniformly distributed current, such as the one in the armature slot of a dc motor. Next, by applying the integral results in Eqs. (12), (13) and (14) and completing Ampere's circuital law around node i, the following nodal equation is obtained:

$$h_i = f_i - g_i \, \partial A_i / \partial t, \tag{16}$$

where

$$h_i = \oint_c \boldsymbol{H} \cdot d\boldsymbol{l} = \sum_{e=e_1}^{e_n} \frac{\nu_e}{2D_e}\left\{\sum_{m=i}^{k} (c_{i,e} c_{m,e} + b_{i,e} b_{m,e}) A_{m,e}\right\}, \tag{17}$$

$$f_i = \int_s J_s dxdy = \sum_{e=e_1}^{e_n} J_{se} S_{i,e}, \tag{18}$$

$$g_i = \int_s \sigma dxdy = \sum_{e=e_1}^{e_n} \sigma_e S_{i,e}. \tag{19}$$

In the equations, $b_{i,e}$, $c_{i,e}$, $A_{m,e}$ and $S_{i,e}$ are b_i, c_i, A_m and S_i of the e_r $-th (r = 1, 2, \cdots n)$ element around node i.

In Eq. (16), there is contained the time derivative $\partial A_i/\partial t$. Therefore, in order to numerically solve the equation, we apply the Crank-Nikolson finite difference method to $\partial A_i/\partial t$, by which a sufficiently accurate approximation of a time derivative can be obtained. When the value of A_i at time t is evaluated, the value at $t + \Delta t$ is given by the following equation[6]:

$$(A_i)_{t+\Delta t}=(A_i)_t+\Delta t\left\{\varepsilon_i\left(\frac{\partial A_i}{\partial t}\right)_{t+\Delta t}+(1-\varepsilon_i)\left(\frac{\partial A_i}{\partial t}\right)_t\right\}, \tag{20}$$

where ε_i is a weight factor of the time derivative and $0\leq\varepsilon_i\leq 1$. From Eqs. (16) and (20), we can get

$$(g_iA_i+\varepsilon_i\Delta th_i)_{t+\Delta t}=\{g_iA_i-(1-\varepsilon_i)\Delta th_i\}_t+\Delta t\{\varepsilon_i(f_i)_{t+\Delta t}+(1-\varepsilon_i)(f_i)_t\}. \tag{21}$$

This is the final form of a discrete nodal equation for node i, where $\varepsilon_i=1$ for node of $g_i=0$.

Here, let us consider the nodal equation for node i which exists on the boundary, as shown in Fig. 3, (a) and (b). On a boundary where the normal component B_n of $\boldsymbol{B}$ is zero, $A=A_i$ does not vary by the coordinates x and y. On another boundary where the tangential component H_t of $\boldsymbol{H}$ is zero, $\partial A/\partial n=0$ is satisfied and the nodal equation is derived from integrating Eq. (11) in an incomplete circuital integral region, as shown in Fig. 3 (b).

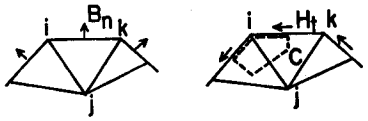

(a) $B_n=0$ (b) $H_t=0$

Fig. 3. Boundary conditions.

Finally, from Eq. (21) and the given boundary conditions about B_n or H_t, the nonlinear simultaneous nodal equations for all nodes are derived as follows:

$$([\boldsymbol{G}]+\Delta t[\boldsymbol{\varepsilon}][\boldsymbol{H}])[\boldsymbol{A}]_{t+\Delta t}=\{[\boldsymbol{G}]-\Delta t([\boldsymbol{U}]-[\boldsymbol{\varepsilon}])[\boldsymbol{H}]\}[\boldsymbol{A}]_t$$
$$+\Delta t\{[\boldsymbol{\varepsilon}][\boldsymbol{F}]_{t+\Delta t}+([\boldsymbol{U}]-[\boldsymbol{\varepsilon}])[\boldsymbol{F}]_t\}, \tag{22}$$

in matrix form, where

$$[\boldsymbol{A}]=\begin{bmatrix}A_1\\A_2\\\vdots\\A_i\\\vdots\\A_n\end{bmatrix},\quad [\boldsymbol{F}]=\begin{bmatrix}f_1\\f_2\\\vdots\\f_i\\\vdots\\f_n\end{bmatrix},\quad [\boldsymbol{G}]=\begin{bmatrix}g_1&&&&\boldsymbol{O}\\&g_2&&&\\&&\ddots&&\\&&&g_i&\\&&&&\ddots\\\boldsymbol{O}&&&&g_n\end{bmatrix},$$

$$[\boldsymbol{H}]=\begin{bmatrix}h_{11}&h_{12}&\cdots\cdots&h_{1n}\\h_{21}&h_{22}&&\vdots\\\vdots&&h_{ii}&\vdots\\h_{n1}&\cdots\cdots&\cdots\cdots&h_{nn}\end{bmatrix},\quad [\boldsymbol{\varepsilon}]=\begin{bmatrix}\varepsilon_1&&&&\boldsymbol{O}\\&\varepsilon_2&&&\\&&\ddots&&\\&&&\varepsilon_i&\\&&&&\ddots\\\boldsymbol{O}&&&&\varepsilon_n\end{bmatrix},$$

$$[\boldsymbol{U}]=\begin{bmatrix}1&&&\boldsymbol{O}\\&1&&\\&&1&\\&&&\ddots\\\boldsymbol{O}&&&1\end{bmatrix}. \tag{22'}$$

In these equations,

n : total number of nodes,

$[\boldsymbol{A}]$: row matrix constructed with unknown vector potential at all nodes,

$[\boldsymbol{G}]$: diagonal coefficient matrix derived from Eq. (19) and the given boundary conditions,

$[\boldsymbol{H}]$: nonlinear and sparse coefficient matrix derived from Eq. (17) and the boundary conditions,

$[\boldsymbol{F}]$: row matrix derived from Eq. (18).

$[\boldsymbol{\varepsilon}]$: diagonal matrix constructed with ε_i,

$[\boldsymbol{U}]$: unit matrix,

By numerically solving Eq. (22), the transient value of A at each node is obtained, and subsequently, the transient response and distribution of the magnetic flux, etc. can be evaluated. In this connection, for firstly solving Eq. (22), an iterative procedure is needed, and by using the successive relaxation and the sweep out methods, the repetition time can be fairly decreased.

3. Magnetic Circuit Model to Investigate the Interpole Flux

We apply our numerical nodal method to investigate the transient response of the interpole flux in a dc motor in a case where an armature current abruptly changes. Now, for simplifying the analysis, we introduce the magnetic circuit model by which the transient response of the interpole flux may be accurately investigated. In Fig. 4, the magnetic paths containing the interpole are shown by the broken lines. In the figure, let us assume that the influence on the interpole flux by the main pole, the armature slots and the leakage flux can be neglected, the following magnetic equation is obtained:

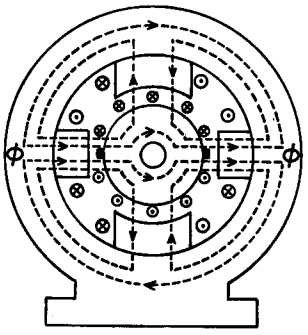

Fig. 4. Simplified distribution of interpole flux in dc motor.

$$AT_i - AT_a = (R_a + R_g + R_i + R_y)\,\phi, \tag{23}$$

where

AT_i : mmf due to interpole exciting current,

AT_a : counter mmf for interpole flux due to armature current,

R_a, R_g, R_i and R_y : magnetic reluctance of armature, interpole air gaps, interpoles and yoke, respectively,

ϕ : magnetic flux in interpole.

The magnetic circuit model shown in Fig. 5 has been derived from Eq. (23), in a case where the armature and the yoke were constructed with laminated cores and the interpole with a solid core. In this case, the analysis of the transient response of the interpole flux is already achieved[7),8)]. However, the usual dc motor has a yoke constructed with a solid core and the interpole with a laminated core, so another model, one such as is shown in Fig. 6, must be used. In Figs. 5 and 6, A_r, G_a, I_p and Y_o correspond to the armature, the interpole air gap, the interpole and the yoke, respectively, and W is an exciting winding which prepares the mmf AT_i-AT_a.

In Fig. 7, there is shown the magnetic circuit model to be used for an experimental investigation of the transient response of the magnetic flux and for examining the validity of our numerical calculation. In the figure, A_r and I_p are constructed

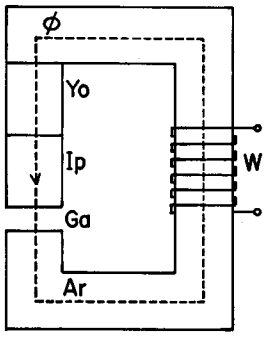

Fig. 5. Conventional magnetic circuit model.

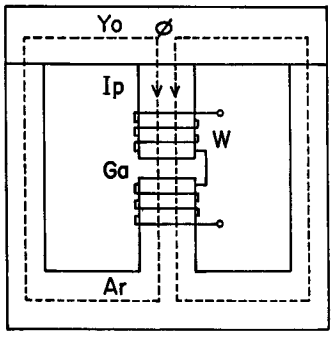

Fig. 6. Magnetic circuit model considering yoke constructed with solid iron.

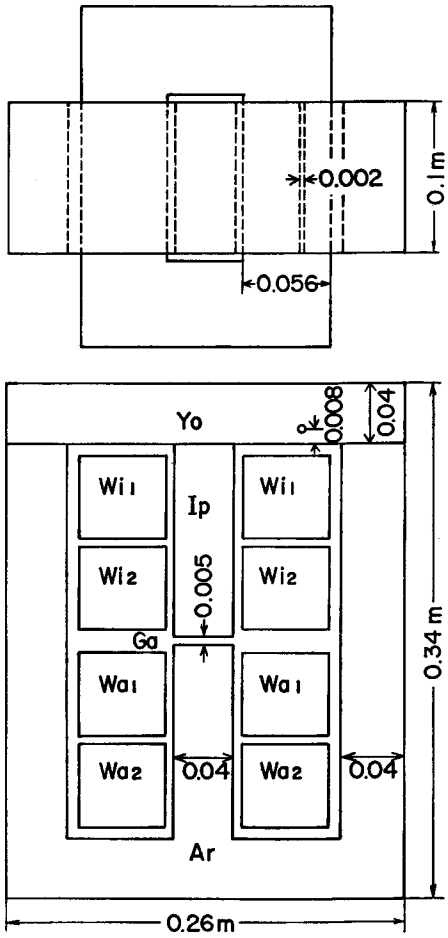

Fig. 7. Prepared magnetic circuit model.

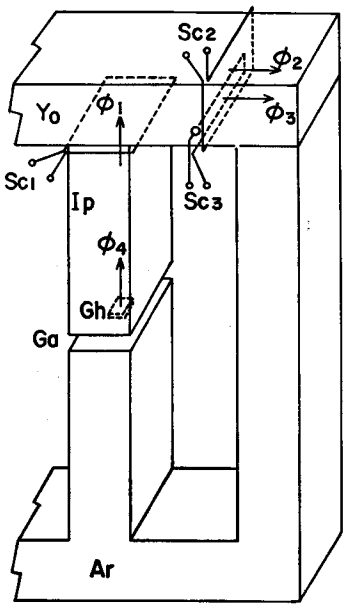

Fig. 8. Settlement of search coils and hall cell.

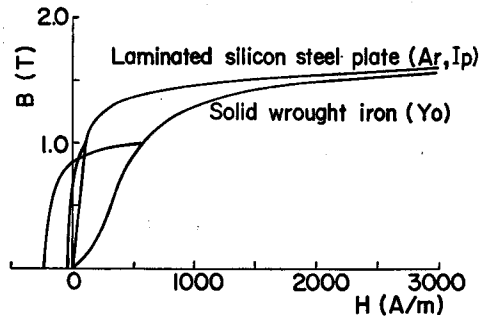

Fig. 9. Magnetization curves.

with laminated silicon steel plates, and Y_o with solid wrought iron. There are four windings, W_{i1}, W_{i2}, W_{a1} and W_{a2}, which are bound by 2000 turns to supply the mmf AT_i and AT_a in Eq. 23, respectively. Moreover, there are set some search coils S_{c1}, S_{c2} and S_{c3} and the hall cell G_h, as shown in Fig. 8, to record the transient response of the magnetic flux. The $B-H$ magnetization curves of the used cores are shown in Fig. 9. In this figure, the representative hysteresis curves are also shown.

4. Calculated and Experimental Results

4.1 Experimental circuit

Figure 10 shows a schematic diagram of the experimental circuit, in which an exciting current I is suddenly supplied to the windings W_{i1}, W_{i2} and W_{a1} from the direct current source voltage E by closing the switch S. The magnitude and time constant of I are varied by changing E and the resistance R. Then, the transient response of fluxes ϕ_1, ϕ_2 and ϕ_3 are measured by integrating the voltages induced in the search coils S_{c1}, S_{c2} and S_{c3}, respectively. The flux ϕ_4 is evaluated by multiplying the cross-sectional area $(0.04\times 0.1\text{m}^2)$ of G_a by the magnetic flux density measured with the hall cell G_h. Here, the fluxes

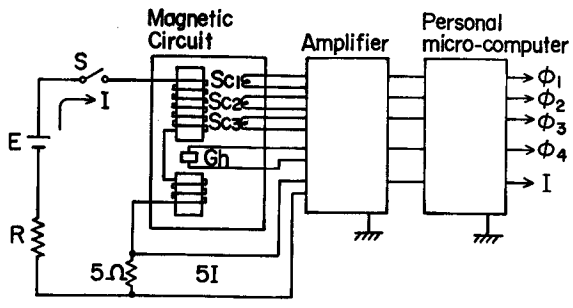

Fig. 10. Schematic diagram of experimental circuit.

ϕ_1 to ϕ_4 correspond to the fluxes through the interpole core, the yoke core, the inner part of the yoke core and the interpole air gap, respectively, of the dc motor.

The experiment must start after residual magnetism in the magnetic circuit model is sufficiently weakened. The measured data are processed with a personal microcomputer.

4.2 Boundary conditions and assumptions for numerical calculation

The transient response of the magnetic flux, the distributions of the magnetic flux, and also the eddy current in the magnetic circuit model shown in Fig. 7 are calculated under the following assumptions.

(1) The two-dimensional analysis is carried out in the field region, as shown in Fig. 11, where $\overline{OP_3}$ is a center line of the cross-section, and the magnetic flux distributes symmetrically with respect to the line. In the figure, the leakage fluxes from the boundary lines $\overline{OP_1}$, $\overline{P_1P_2}$ and $\overline{P_2P_3}$ are assumed to be negligible. The field region is subdivided into many triangular elements, as shown in Fig. 12.

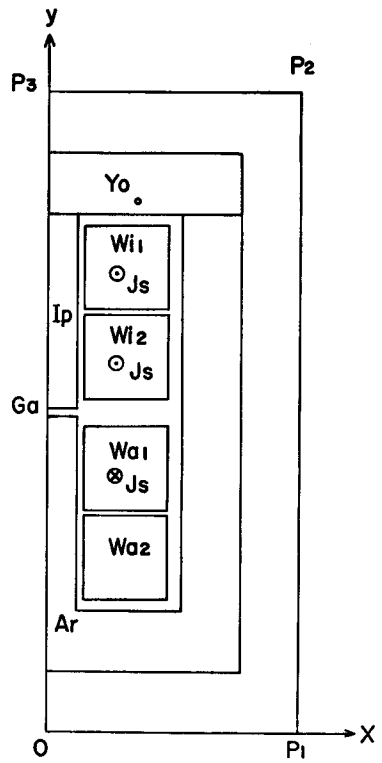

Fig. 11. Cross-sectional view to investigate flux distribution.

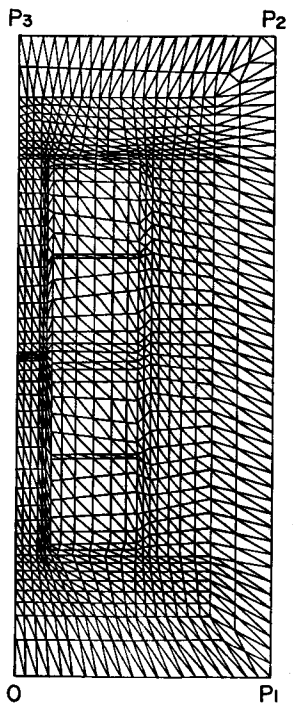

Fig. 12. Mesh of triangles for nodal method.

(2) In the magnetic circuits I_p and A_r constructed with laminated cores, the induced eddy current can be neglected, and so the conductivity is assumed to be zero. The conductivity $\sigma=\sigma_y$ of Y_e constructed with a solid core is assumed to be uniform.

(3) It is assumed that the current density J_s in the exciting windings W_{i1}, W_{i2} and W_{a1} is uniform and $J_s=2000\times I/(0.058\times 0.054m^2)$.

(4) The reciprocal permeability ν_e in Eq. (17) is assumed to be approximated by the following Frölich formula

$$\nu_e=\frac{H_e}{B_e}=\frac{\eta_e}{1-\xi_e B_e}+\frac{H_e}{B_e}, \tag{24}$$

where η_e, ξ_e and H_e are the coefficients determined by the magnetization curve of the material in element e, as shown in Fig. 13. Also, we express the hysteresis characteristic shown in the figure by a simular formula.

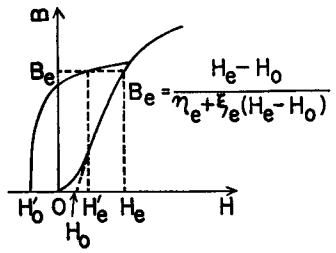

Fig. 13. Frölich formula to obtain reciprocal permeability.

Next, let us consider the boundary conditions on the boundary lines $\overline{OP_1}$, $\overline{P_1P_2}$ and $\overline{P_2P_3}$ in Fig. 12. From the assumption (1), the normal component B_n on the lines vanishes. Also, we can put $B_n=0$ on line $\overline{OP_3}$. Then, on those lines, we have $A=A_e$ which is independent of x and y. Furthermore, the additional constraint to A_e is given as follows:

$$\sigma_y\,\partial A_e/\partial t=0 \tag{25}$$

on line $\overline{OP_3}$ on which the eddy current must be zero. Accordingly, A_e becomes independent on t, too, and so we put $A_e=0$ for simplifying the analysis.

4.3 Results and discussions

The experimental responses of the current and the fluxes are shown in Fig. 14 (a), when the switch S is suddenly closed, as shown in Fig. 10, where $T_m=0.051$ s is a measured time constant of I. In the figure, a ripple is seen in the waveform of ϕ_4, which is caused by the characteristic of the hall cell G_h. In Fig. 14(b), the calculated results by Eqs. (8) and (22) are shown, where $I=0.5\times(1-\exp(-t/T_m))$ A and $\sigma_y=1MS/m$. Though the actual magnetic flux is distributed in the three-dimensional space, the calculations by our two-dimensional analysis agree fairly well with the experimental ones. In the figures, the relations $\phi_4\ll\phi_1$ and $\phi_2\fallingdotseq\phi_1/2$ are satisfied. The former relation shows that the fairly large leakage flux occurs at the side surfaces of I_p, and the latter relation denotes that the leakage flux from the side surfaces of Y_e

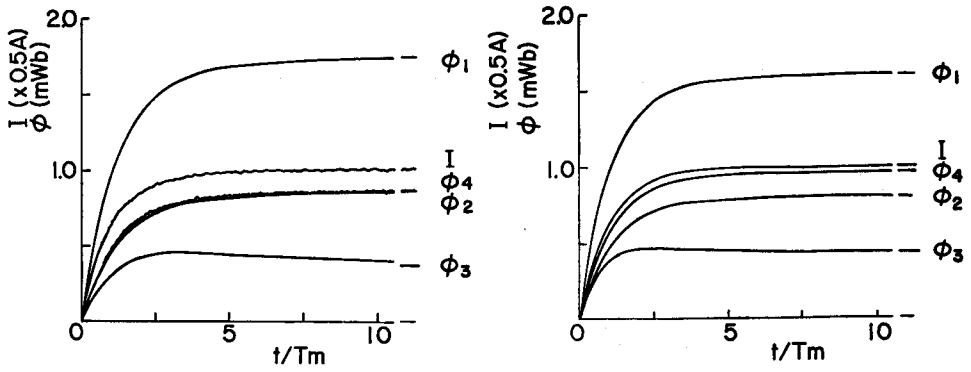

(a) Experimental results (b) Calculated results

Fig. 14. Transient response of magnetic flux for $T_m=0.051s$ and $\sigma_y=1$ MS/m.

is small. We can also see that the relation $\phi_3 \fallingdotseq \phi_2/2$ is satisfied in Y_o immediately after I is supplied and this relation is apt to be kept in the steady state where the induced eddy current vanishes. This phenomenon is thought to be caused by the early eddy current induced in Y_o and the magnetic hysteresis.

In Fig. 15, (a) to (d), the calculated flux distributions at $t=T_m/2$, T_m, $5T_m$ and in the steady state ($t\to\infty$) are shown, where ΔA_{eq} is a contour interval of A between neighbouring equi-vector potential lines, which are flux lines. Figure 16, (a) to (d), shoms the distributions of the magnetic flux density corresponding to Fig. 15, (a) to (d), respectively. Also, the distributions of the induced eddy current which correspond to Fig. 15, (a) to (c), are shown in Fig. 17, (a) to (c), where the eddy current is approximately calculated by $\sigma_y \partial A/\partial t$.

It is made clear from Figs. 15, 16 and 17 that the magnetic flux through Y_o constructed with a solid core inclines to concentrate near the inner surface of Y_o by the induced eddy current and the magnetic hysteresis. Therefore, the conventional analysis, using the linear theory and the magnetic circuit model in Fig. 5, is inadequate to analyse the transient magnetic flux in a dc motor whose yoke is constructed with a solid core.

In Fig. 18, (a) and (b), there are shown the experimental and calculated results of the transient response of the fluxes ϕ_1 to ϕ_4 for $T_m=0.116$ s. In the figure, there is seen a fairly good agreement between both results, as well as in Fig. 14. The fluxes ϕ_1 to ϕ_4 respond merely faster to I than those in Fig. 14. We can also see that the ratio ϕ_3/ϕ_2 is somewhat lower than that in Fig. 14, because the eddy current induced in Y_o becomes small.

Next, let us investigate the influence of σ_y on the transient response of fluxes.

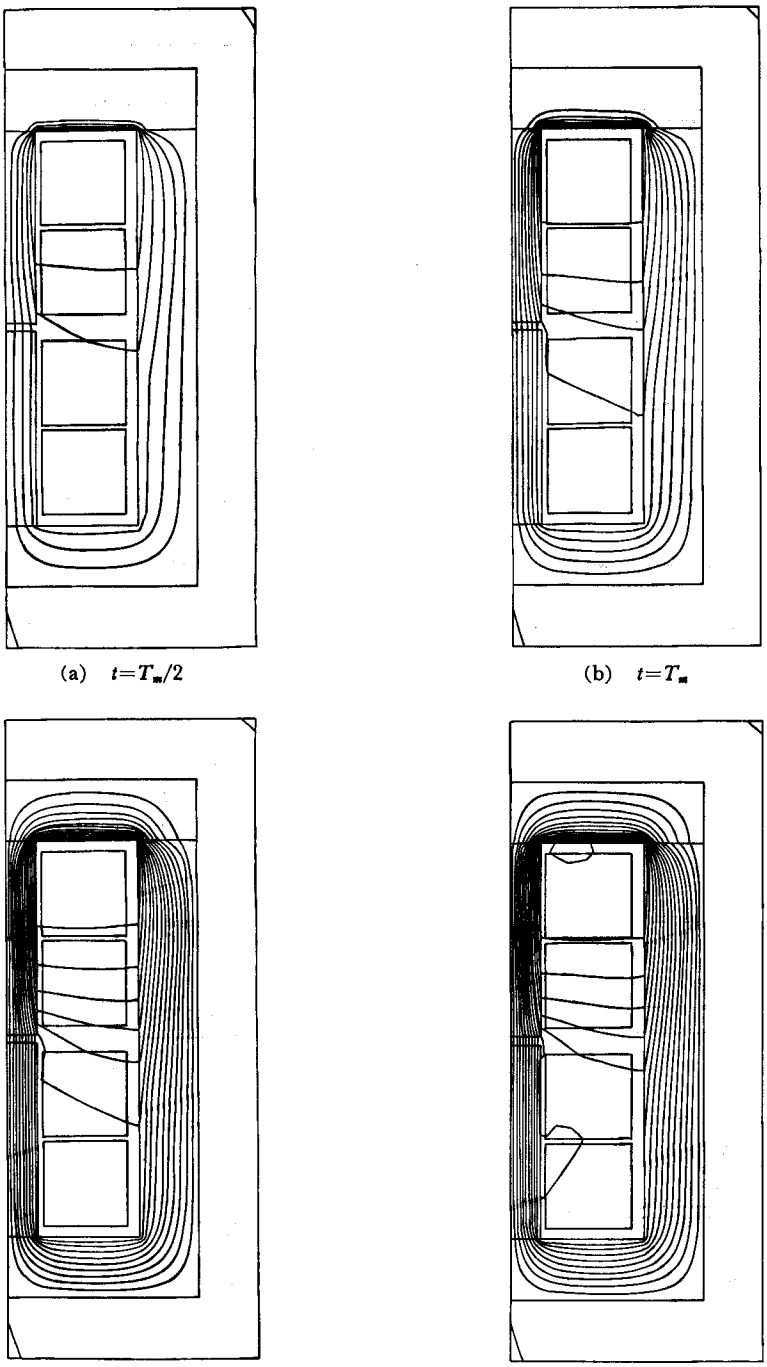

(a) $t=T_m/2$ (b) $t=T_m$

(c) $t=5T_m$ (d) $t\to\infty$

Fig. 15. Flux distributions for $T_m=0.051$ s, $\sigma_y=1MS/m$ and $\Delta A_{st}=0.5$ mWb/m.

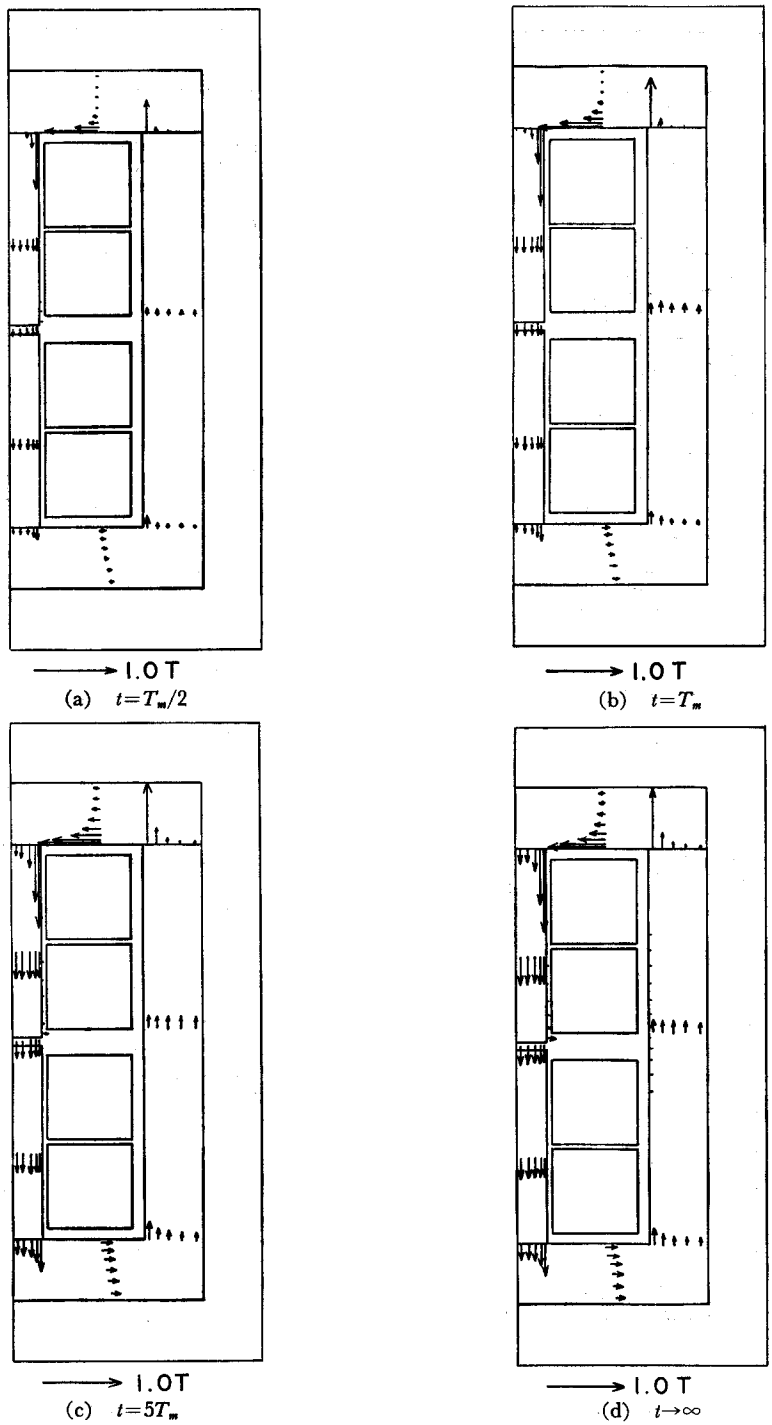

Fig. 16. Distributions of magnetic flux density for $T_m=0.051\,s$ and $\sigma_y=1\,MS/m$.

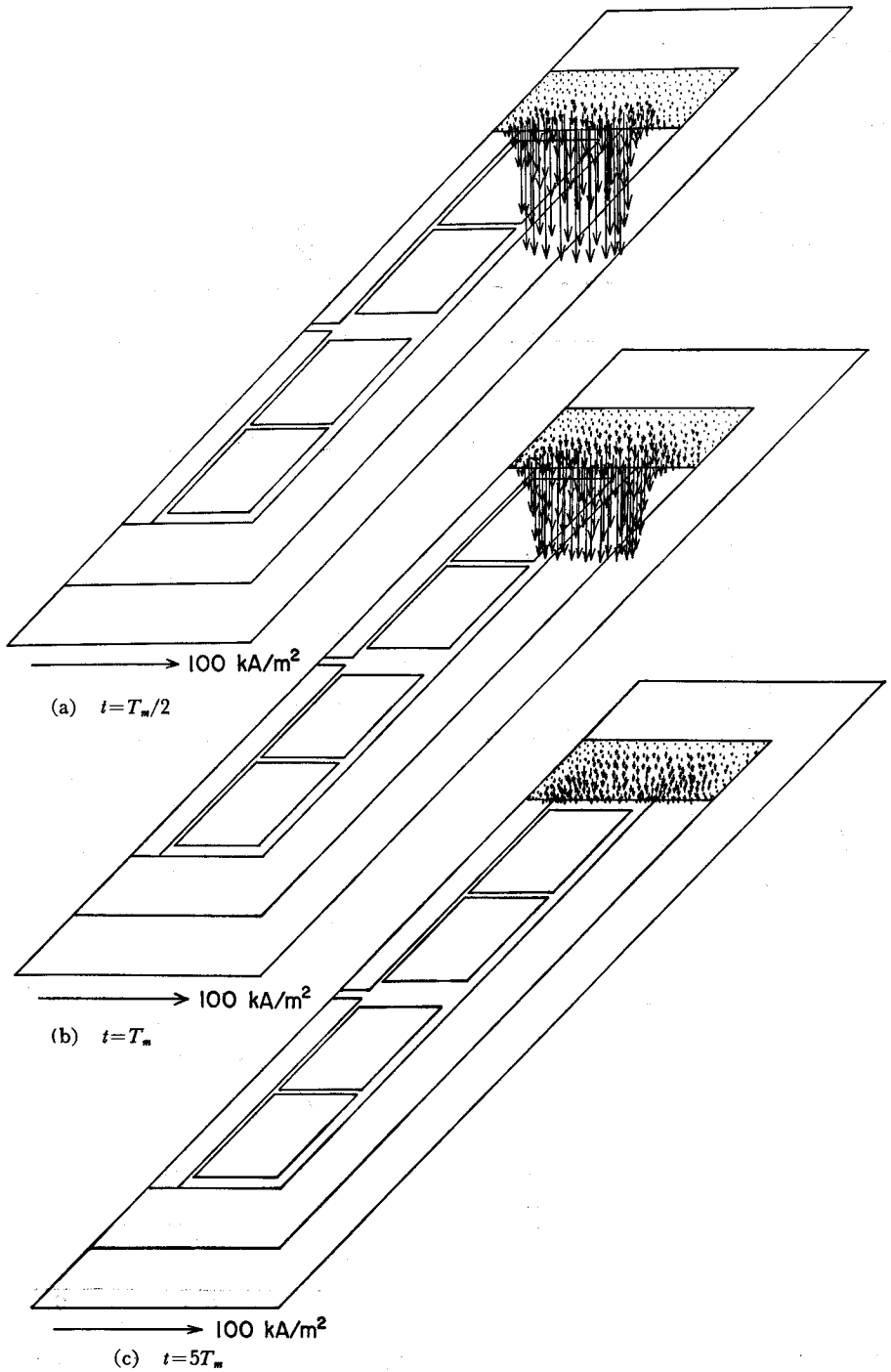

Fig. 17. Distributions of induced eddy current for $T_m=0.051\,s$ and $\sigma_y=1\,MS/m$.

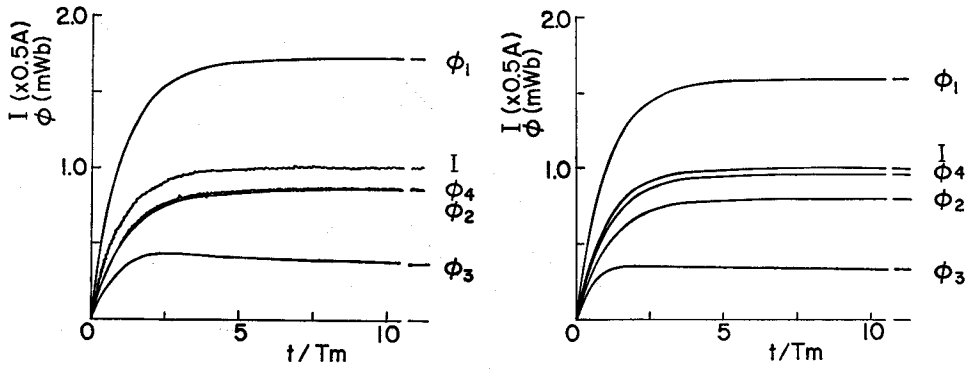

(a) Experimental results (b) Calculated results

Fig. 18. Transient response of magnetic flux for $T_m=0.116\,s$ and $\sigma_y=1\,MS/m$.

The calculated results for $T_m=0.051\,s$ and $\sigma_y=0$, 1 and 5 MS/m are plotted in Fig. 19. In the figure, the fluxes for $\sigma_y=0$ respond to I without the delay time and ϕ_3 approaches closely to $\phi_2/5$, because the eddy current is not induced. Therefore, the magnetic flux is apt to be uniformly distrbuted in Y_o.

Finally, we make clear that the magnetic hysteresis has a large influence on the flux distribution in the yoke of a dc motor. In Fig. 20, the transient response of the magnetic fluxes for $T_m=0.051\,s$ and $\sigma_y=1\,MS/m$ are shown in two cases, one where the magnetic hestersis is taken into consideration, and the other where it is not considered. Till $t\fallingdotseq 2T_m$, when the fluxes ϕ_3's in both cases pass their maximum values, the ϕ_3's are nearly equal to each other. In the former case, for $t>2T_m$, ϕ_3 decreases only a little, and that agrees well with the experimental result. However, ϕ_3 in the latter case decreases with the lapse of time and approaches closely to $\phi_2/5$ in the

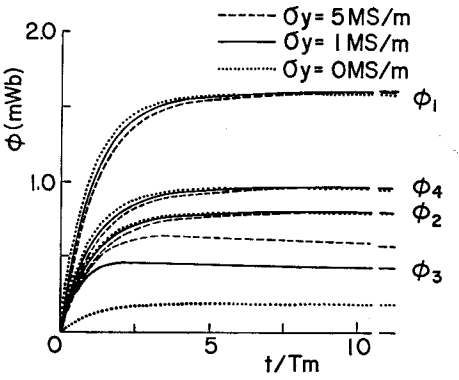

Fig. 19. Influence of σ_y on transient response of magnetic flux.

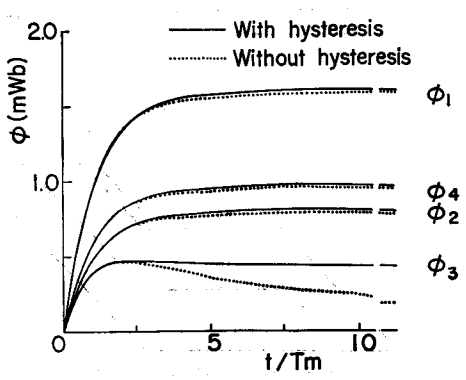

Fig. 20. Influence of magnetic hysteresis on transient response of magnetic flux.

steady state, as well as ϕ_3 for $\sigma_y=0$ in Fig. 19.

5. Conclusions

We formulated a numerical method to solve the two-dimensional theoretical equations for an analysis of the transient response of the magnetic flux in an electric machine. In the numerical calculation, the nodal method considering Ampere's circuital law in the $x-y$ plane and the Crank-Nicolson method for the time derivative are used.

Next, we investigated the transient response of the magnetic flux, the distributions of the magnetic flux, the induced eddy current, etc. in the magnetic circuit which simulates appropriately the interpole circuit in a dc motor, the yoke of which is constructed with a solid iron core.

We could obtain a fairly good agreement between the calculated and the experimental results of the flux response in a case where the magnetic circuit is suddenly magnetized by an exciting current. From the calculated distributions of the magnetic flux and the eddy current, it has been verified that the large magnetic flux and eddy current concentrate for the initial duration in the inner skin region of the yoke. Also, it was verified that the magnetic flux keeps its magnitude after the lapse of the time till steady state, because of the magnetic hysteresis. These factors cause a time delay of the interpole flux in a dc motor and have a bad influence on the commutation. Furthermore, it has been made clear that the conductivity of the yoke and the magnetic hysteresis have a great influence on the flux distribution in the yoke.

References

1) R, Ründenberg: 'Transient Performance of Electric Power System', McGraw-Hill, Inc., New York, p106 (1950).
2) J. Švajcr: IEEE Trans. on Mag., **Mag-10**, 54 (1974).
3) Y. Matsushima, H. Fujiwara et al.: Technical Group. Rotating Machine. IEE. J. Japan, **RM-80-4** (1980).
4) N. A. Demerdash and D. H. Gillot: IEEE Trans. on Mag., **Mag-10**, 682 (1974).
5) A. Y. Hannalla and D. C. Macdonald: IEEE Trans. on Mag., **Mag-11**, 1544 (1975).
6) G. D. Smith (Translated by Y. Fujikawa): 'Numerical Solution of Partial Difference Equations', Sciencesha, Ltd., Japan, p17 (1977).
7) S. Sakabe, T. Nomura and M. Iwamoto: Trans. IEE. Japan, **97-B**, 279 (1977).
8) T. Ando and J. Umoto: Trans. IEE. Japan, **100-B**, 492 (1980).